ZANCO Journal of Pure and Applied Sciences

TYPE Original article
DOI http://dx.doi.org/10.21271/ZJPAS.37.3.4

Removal of Antibiotic Drugs from Aqueous Solution by Modified Coconut Shell

Rekan M. Saeed* ,Rounak M. Shariff

Department of Chemistry, College of Science, Salahaddin University- Erbil, Erbil, Kurdistan Region, Iraq

OPEN ACCESS

*Corresponding author

Rekan M. Saeed

rekan.saeed @su.edu.krd

RECEIVED :23 /12 /2024
ACCEPTED :08/04/ 2025
PUBLISHED :30/ 06/ 2025

KEYWORDS:

activated carbon; adsorption; antibiotic; Nickel (II) oxide nanoparticles; thermodynamics.

ABSTRACT

In this study, coconut shell (CS), coconut shell carbonized (CSC), acid coconut shell carbonized (ACSC), base coconut shell carbonized (BCSC) finally coconut shell carbonized impregnation by nickel (II) oxide (CSC/NiO) nanocomposite, investigated to remove ciprofloxacin (CIP) from an aqueous solution. Optimization of adsorption conditions: initial CIP concentration, pH, adsorbent dose and contact time were studied and found to have a significant effect on CIP removal. The morphological and chemical characteristics of the adsorbents were established by Fourier Transform Infrared (FTIR), X-Ray diffraction (XRD), The Scanning Electron Microscopy (SEM) and Energy Dispersive X-Ray (EDX). The adsorption kinetic study shows the CIP adsorption onto adsorbents follow the pseudo-second order, the values of K_2, q_e and R^2 in the range (0.254-9.529) $g\mu g^{-1}min^{-1}$, (0.016-0.300) mgg^{-1} and (0.706-0.980) respectively at three different temperature 298 K, 308 K and 318 K. The Freundlich isotherm model adsorption data were applied and the value of K_F, n_F and R^2 in the range (3.056-3.694) **mg g^{-1}**, (1.379-1.720) and (0.886-0.999) respectively. The experimental data found to be suitable linearity with Langmuir isotherm the value of K_L, C_m and R^2 in the range (0.011-0.180) L mg^{-1}, (10000-166667) **µg** g^{-1} and (0.760-0.980) respectively. The negative values of ΔG^o (−18.47 to −23.74) kJ mol^{-1} and positive value of each of ΔH^o and ΔS^o in the range (0.131 to 0.228) kJ mol^{-1} and (0.992 to 1) kJ $mol^{-1}K^{-1}$ were indicating the adsorption of CIP on to adsorbents was a spontaneous and endothermic process.

1.Introduction

Presence of antibiotics in the environment especially in aquatic ones is considered a major concern. These antibiotics are used to improve the health of human and livestock and to raise the growth in fish and livestock farms(Samarghandi et al., 2019)Antibiotics posing adverse effects on aquatic ecosystems, the most often absorbed pollutants include medications, antibiotics and contaminated water sources, which have recently drawn a lot of attention. (Azizi, 2021). The most common classification of antibiotics is based on their mode of action, which includes fluoroquinolones, quinolones, *β*-lactams, sulfonamides, monobactams, carbapenems and aminoglycosides. Quinolones (ciprofloxacin, levofloxacin, ofloxacin and norfloxacin) are broad-spectrum antibiotics that are widely prescribed (de Ilurdoz et al., 2022). CIP stands in the first of antibiotics prescribed in this group, a second-generation fluoroquinolone antibiotic, it has a fluorine atom at position 6 in the quinolone group to target most gram-negative and some gram-positive bacteria (Falyouna et al., 2022). CIP prevents the replication of bacteria (caused by Gram-negative and Gram-positive), its wide consumption as a broad spectrum drug and the biodegradation resistance (Igwegbe et al., 2021). CIP has a high solubility in aqueous media and high sustainability in soil and effluent systems at different pH conditions (Jiang et al., 2013). CIP removable from aqueous solution done by several physicochemical processes such as ozonation (Alsager et al., 2018), photocatalytic processes (Hassani et al., 2018), adsorption (Malakootian et al., 2018), electro-Fenton, electrocoagulation (Yahya et al., 2014) and magnetic nanomaterials (Chang et al., 2021).

CS which is one of the most biomass wastes: husk, frond, fiber and pulp (Ayrilmis et al., 2011). It is regarded that CS is one of the ideal raw materials with natural structure for preparing porous materials and low ash content (Yahya et al., 2015). CS widely used for removal of a variety water pollutants because of abundant functional groups and high specific surface area (Su et al., 2003). Many modification methods have been evaluated to improve the adsorption capacity of CS such as thermal treatment, chemical functionalization, hetero-atom doping and composites with metal (hydro) oxides (Kuśmierek et al., 2017). There are many recent publications about the effect of carbonization or activation temperature during the preparation of adsorbents on adsorption (Chen et al., 2020). The adsorption characteristics of a carbon-based adsorbent are known to be dependent not only on the surface area but also on the functional groups and the properties of graphitic structures (Zhu et al., 2021). Since the adsorption of organic compounds on them is largely attributed to electrostatic attraction, hydrophobic interaction and electron donor-acceptor interactions (Peng et al., 2016, Zheng et al., 2021). The enhanced adsorptive capacity with physical modification and chemical activation enhances the surface area due to the shorter activation time and lower activation energy of functionalized porous carbons in the presence of an alkaline or acid activation agent (Panahi et al., 2020). Pseudo-second-order and Langmuir equations were applied to the adsorption process under the optimized conditions, the maximum absorption capacity in modified cellulose of Pb^{2+} was 58.3 mg/g. (Ibrahim et al., 2024).The Langmuir isotherm model, second-order reaction and thermodynamic characteristic adsorption process was an endothermic spontaneous process (Sharef et al., 2023) The resultant was characterized by FTIR, UV–Vis, XRD and SEM devices. The pseudo-second-order and Freundlich equations was applied to the adsorption process (Ibrahim and Fakhre, 2019). The adsorption parameters, such as pH, adsorbent dose, contact time, initial metal ion concentration and temperature were optimized. The regeneration of the adsorbents depends on the type and concentration of the regenerating solution. (Fakhre and Ibrahim, 2018)

The efficiency of modified coconut shell biosorbents for promoting economic and environmental viability in purifying contaminants such as antibiotic drugs in environment. The high level of consumption of antibiotics in both human and veterinary cause a risk to the food chain and water bodies which affect the living organisms. Water and wastewater treatment impotent to

resume healthy live so in this study modified coconut shell prepared to obtain effectively remove CIP from an aqueous solution. The adsorbents were characterized regarding their pore structure and surface properties. This study investigated the potential of modified coconut shell for CIP removal from aqueous solutions using batch adsorption experiments. The CIP adsorption process parameters such as initial CIP concentration, pH, adsorbent dosage and contact time were optimized employing response surface methodology. Adsorption kinetics, isotherm and thermodynamic studies were conducted to describe the removal mechanism and nature of CIP adsorption with modified coconut shell. Furthermore, an adsorbent reuse and recycle test was conducted for four consecutive CIP adsorption-desorption cycles.

2. Materials and Methods

2. 1. Chemicals and equipments

Materials used in this research: antibiotics CIP from Quinolone groups of antibiotics were selected for adsorption studies. 97.5% Ciprofloxacin hydrochloride (Copran, Ajanta-India). Boric acid (H_3BO_3) 99% from (BDH), Sodium chloride (NaCl) and methanol (99% purity) was purchased from (TEDIA-USA), Sulfuric acid (98%, Sp.gr.1.84) from (Barcelona-Spain) and Nickel (II)nitrate hexahydrate [$Ni(NO_3)_2.6H_2O$] were purchased from (BDH). sodium hydroxide pellets [NaOH] were acquired from (Sigma-Aldrich, Germany). All chemicals and reagents were locally acquired and used without further purification.

The study used various instruments to analyze the including a UV-Visible spectrophotometer, a pH meter, XRD patterns, FTIR spectra, SEM and EDX pictures.

2.2 Adsorbat

Ciprofloxacin hydrochloride, also known as 1-cyclopropyl-6-fluoro-4-oxo-7-piperazin-1-yl-quinoline-3carboxylic acid, is a quinolone with a molecular weight of 367.8 gm/mol and a pK_a value is 8.76 (Azizi, 2021). The value of pH around (3-4.5). The structures of the studied antibiotic were represented in Figure 1.

A 1000 mgl^{-1} aqueous stock solution of CIP was prepared, refrigerated and diluted to various concentrations. Calibration curves were detected at 273 nm (Jiang et al., 2013).

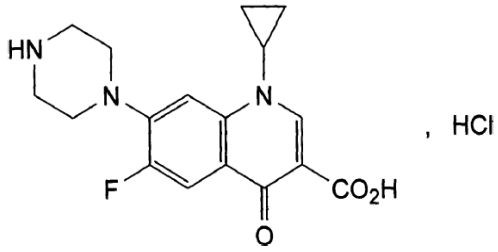

Figure 1 The chemical structure of ciprofloxacin hydrochloride

2.3 Adsorbents

2.3.1 Modified Coconut Shell

CS were cleaned, air dried, crushed, sieved, heated, soaked and sealed to prevent moisture resorption and ensuring a broad surface area for dehydration (Namasivayam et al., 2001).

CSC obtained by take 100 grams of the selected fraction from CS and then carbonized at 600ºC for 1 h. (Aljeboree et al., 2015).

ACSC obtained by impregnated CS with 0.2 M H_2SO_4 for 24 hours, washing with deionized water, drying at 110˚C and activating at 600˚C for 1 hour (Baig et al., 2020).

BCSC done by dispersing CS in 0.2 M KOH for 24 hours, washing, dried at 110˚C finally activated at 600°C for 1 hour (Baig et al., 2020).

The CSC/NiO nanocomposite was synthesized using the chemical precipitation method. The process involved dissolving Ni (II)) in deionized water, adding powdered CS mixing with sodium hydroxide, filtered, dried and activated at 600 ˚C for 1 hour

(Patra et al., 2018).

2.3.2 The physical and chemical properties of modified coconut shell

The physical and chemical properties of modified coconut shell adsorbents shown in table 1.

Table 1 The physical and chemical properties of modified coconut shell adsorbents.

No	Types of adsorbents	Moister content %	pH	EC µS	TDS mg L^{-1}
1	CS	1.573	5.49	693	413
2	CSC	1.21	11.68	740	445
3	ACSC	1.29	7.72	380	226
4	BCSC	2.06	11.724	423	757

5	CSC/NiO	1.06	11.535	707	420

The Zero Charge Point (pH_{PZC}) is determined by solid addition method for the modified coconut shell adsorbents. The value of pH_{pzc} ranged between (7.2- 7.4) the significance of pH_{PZC} is that a given adsorbent surface will have a positive charge at solution pH values less than the pH_{PZC} and thus be a surface on which anions may adsorb. On the other hand, that adsorbent surface will have a negative charge at solution pH values greater than the pH_{PZC} and thus be a surface on which cations may adsorb (Sousa Neto et al., 2012).

2.4. Batch Adsorptions Experiment procedures

The batch adsorption of CIP from an aqueous solution at 298 K was determined using the optimal standard batch equilibrium technique. Adsorptions of CIP onto various adsorbents were investigated based on starting concentration, pH, dosage and contact duration. UV-vis spectrophotometer measurements were used to study the impact of adsorbent quantity and absorbance at 273 nm. The process was replicated at 308 K, 318 K, and the findings were calculated using the following equation (Rumman et al., 2021).

$$q_e = (C_o - C_e)\frac{V}{W} \quad (1)$$

$$q_t = (C_o - C_t)\frac{V}{W} \quad (2)$$

$$\text{Removal}\% = \frac{C_o - C_e}{C_o} x100 \quad (3)$$

The equilibrium adsorption capacity is represented by q_e (mg g^{-1}), C_o and C_e are initial and equilibrium CIP concentrations (mg L^{-1}) respectively. V is the volume of the solution (L) and W is the dry weight of the adsorbent (g). While the value of adsorption at time t q_t (mg g^{-1}). In order to get values from the CIP, the measurements were taken in triplicates and then the mean values were calculated and used for further analysis.

3. Result and discussion

3.1. Characterization of Adsorbents

The FTIR spectra in Figure 2 shows the modified coconut shell adsorbents CS and CSC (a) before adsorption (b) after CIP adsorption for the bands at 3383.14, (3153.61-3759.26) cm $^{-1}$ and (2312.65 -2980.02) cm $^{-1}$ due to O-H stretching, C=O stretching and C-H vibrations of aliphatic hydrocarbons. The C-H peaks indicate carbonyl groups (Sun et al., 2005).

The band refer to –NO stretch of nitrogen containing compound and –CO stretch of carbonyl compounds was observed at around 1354.03 cm^{-1}, and 1398.39 cm^{-1}, while the band (1222.87-1267.23) cm^{-1}, and (1232.51-1265.30) cm^{-1}. The band positioned at 1174.65 cm^{-1}, 1161.15 cm^{-1}, and 1107cm^{-1} refer to C-C stretching. The band positioned at (1031.92-1070.49) cm^{-1}, 1026.13cm^{-1}refer to –CN stretch of aliphatic amines. The observed band at (960.55-983.70) cm^{-1}, and 950.91 cm^{-1} refers to β-glycolic linkages. The band (812.03-873) cm^{-1} refers to ring stretching or may be originates from the N-H, and ring stretching (Zhang et al., 2002)

The FTIR spectra in Figure 2 of the adsorbent ACSC shows that the band at (3032.10-3836.42) cm^{-1}, 2981.95-2086.98) cm^{-1}, due to the O-H stretching, C-H of aliphatic hydrocarbons.1703.14 cm^{-1}, (1604.77-1665.92) cm^{-1}, 1585.49 cm^{-1}, 1354.03 cm^{-1}, (1222.67-1267.23)cm^{-1} could be attributed to primary and secondary amide or C=O group, C=C bonds, either isolated or conjugated, which is related to the presence of carbonyl groups or aromatic rings, N–H deforming, C=C bending, and C-N stretching, CH_3 in the $NHCOCH_3$ group, and acetates stretching, or nitrate (NO_2) symmetric stretching, and acetyl groups in hemicelluloses vibration respectively. The observed band at 1174.65cm^{-1}, 1070.49cm^{-1}, it was as a result of the stretching of the C-O stretching, or C-C. The observed band at1070.49cm^{-1}, 983.70 cm^{-1}, 812.03 cm^{-1}, (630.72-673.16)cm^{-1}, (532.35-599.86) cm^{-1}, (482.20-499.56)cm^{-1}, excite in both before adsorption processes was attributed to the vibration C-O stretching, stretching of C-H, O-O, and β-glucosidic linkages between the sugar units in hemicelluloses and cellulose, N-H, and ring stretching, SO_3 group, and halogenated compounds stretching respectively(Zhang et al., 2002)

The FTIR spectra of BCSC in Figure 2 shows that the bands at 3365.78cm^{-1}, and (2088.91-

2978.09) cm^{-1}, due to the O-H stretching, C-H of aliphatic hydrocarbons respectively. The bands at 1982.82cm^{-1}, 1703.14 cm^{-1}, (1604.77-1665.92) cm^{-1}, 1585.49 cm^{-1}, 1500.62cm^{-1}, 1354.03 cm^{-1}, (1222.67-1267.23)cm^{-1} could be attributed to primary and secondary amide or C=O group, C=C bonds, either isolated or conjugated, which is related to the presence of carbonyl groups or aromatic rings, N–H deforming, C=C bending, and C-N stretching, CH_3 in the $NHCOCH_3$ group, and acetates stretching, or nitrate (NO_2) symmetric stretching, and acetyl groups in hemicelluloses vibration respectively. The observed band at 1174.65cm^{-1}, 1070.49cm^{-1}, it was as a result of the stretching of the C-O stretching, or C-C. The observed band at1070.49cm^{-1}, 981.77 cm^{-1}, (812.03-873.75)cm^{-1}, 775.38cm^{-1}, 663.51cm^{-1}, (516.92-572.86) cm^{-1}, (466.77-478.35)cm^{-1}, excite in both before adsorption processes was attributed to the vibration C-O stretching, stretching of C-H, O-O, N-H, and ring stretching, SO_3 group and halogenated compounds stretching respectively (Zhang et al., 2002).

The FTIR spectrum of the (CSC/NiO) nanocomposite in Figure 2 shows that the bands at around (3118.90-3934.78)cm^{-1}, 2945.30cm^{-1}, (2872.01-2879.72)cm^{-1}, 2503.60cm^{-1}, 2362.8cm^{-1}, and (2113.99-2289.50)cm^{-1} due to the O-H stretching, C-H of aliphatic hydrocarbons. 1982.82cm^{-1},(1608.63-1693.50)cm^{-1}, 1589.34cm^{-1},1408.04cm^{-1},(1224.80-1282.66)cm^{-1},(1172.72-1176.58)cm^{-1} , 1076.28cm^{-1}, could be attributed to primary and secondary amide or C=O group, C=C bonds, either isolated or conjugated, which is related to the presence of carbonyl groups or aromatic rings, N–H deforming, C=C bending, and C-N stretching, CH_3 in the $NHCOCH_3$ group, and acetates stretching, or nitrate (NO_2) symmetric stretching, and acetyl groups in hemicelluloses vibration respectively (1608.63-1693.50)cm^{-1} were attributed to the C=C stretching either isolated or conjugated, C-N, O–H deformation mode of the water molecule, or carbonyl groups stretching before adsorption. –N=N– stretching, –C–N– stretching ,-C-O, C-C stretching , acetyl groups in hemicelluloses,–S=O– stretching , C–H in-plane bending vibration of the benzene ring appeared before and after adsorption. The observed band at (916.19-985.62)cm^{-1}, (813.96-871.82)cm^{-1}, (702.09-777.31)cm^{-1}, 663.51cm^{-1}, (530.42-563.21)cm^{-1}, 478.35cm^{-1} indicative of the stretching of O-O, C-H, N-H, and ring stretching (Wang et al., 2020).

The adsorbents' positions affected the intensity of C−C and C−O bands, indicating high temperature reaction. Adsorption peaks at 2289.50cm^{-1} and 530.42 cm^{-1} were observed indicating –OH, C-H, C-O, C≡ O, and Ni-O groups involved in CIP removal (Peng et al., 2018, Sun et al., 2005, Zhang et al., 2002)

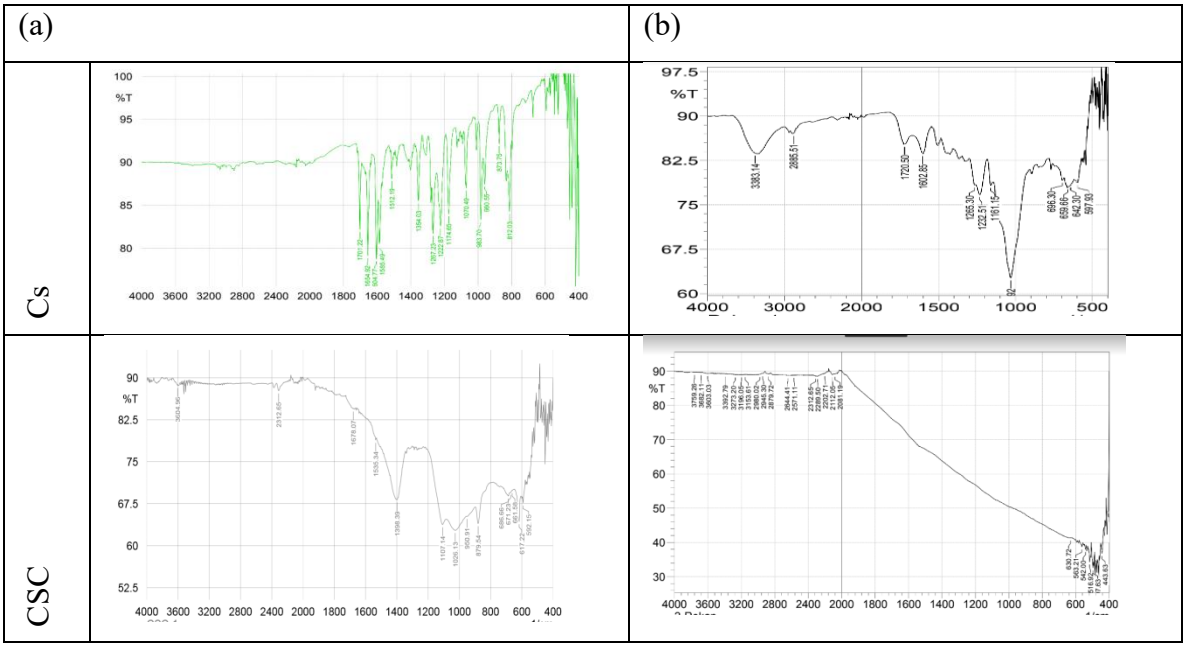

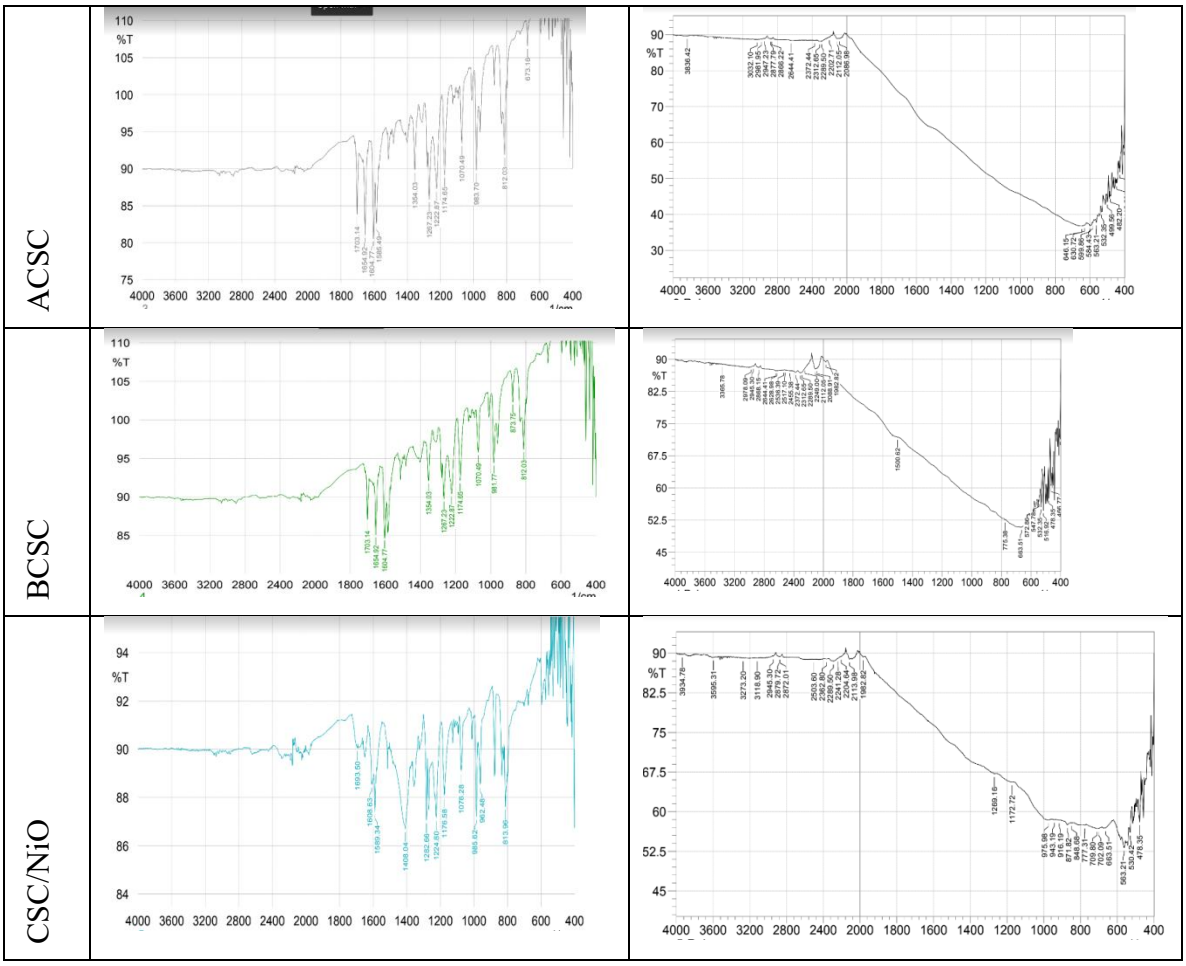

Figure 2: FTIR spectrum of adsorbents (a) before adsorption (b) after adsorption for CIP respectively.

The XRD diffractogram in Figure 3 shows peaks before and after adsorption for CIP in various adsorbents with magnetite peaks at 22º and cubic Ni-O crystallites at 78º respectively indicating their crystalline composition (Al-Musawi et al., 2021). Scherrer's formula accurately calculated average diameter values of metal oxide nanoparticles ranging from 20-40 nm demonstrating excellent accuracy in creating adsorbents with a pristine crystalline structure (Al-Musawi et al., 2021).

(a

CS

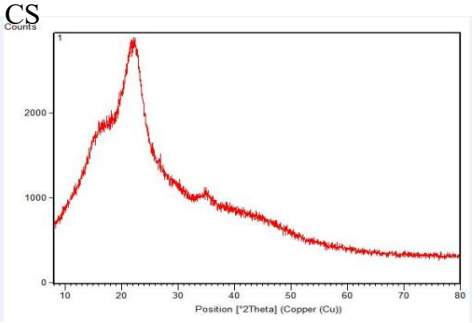

CSC

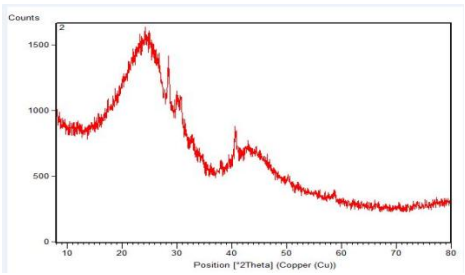

ACSC

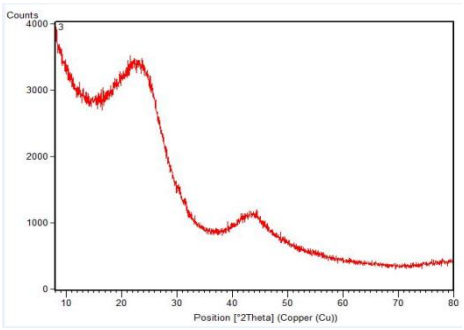

BCSC

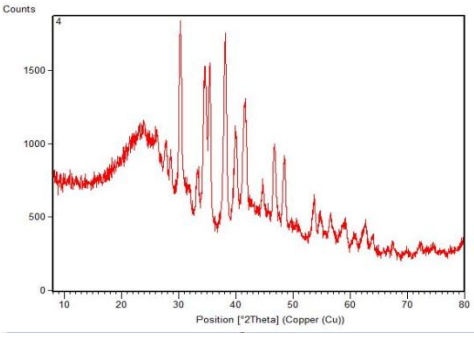

CSC/NiO

(b

CS

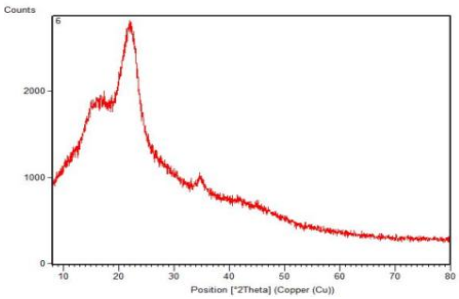

CSC

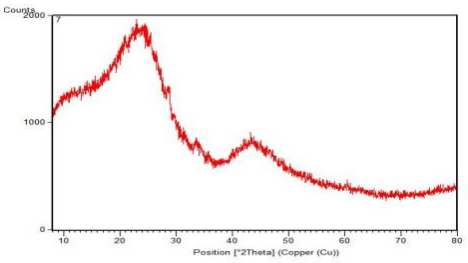

ACSC

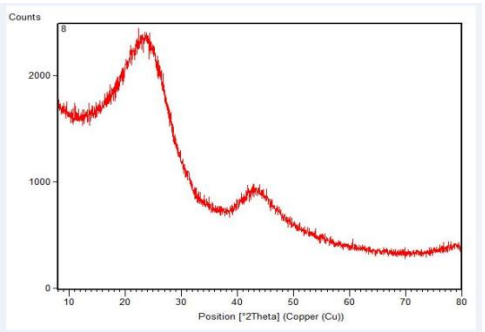

BCSC

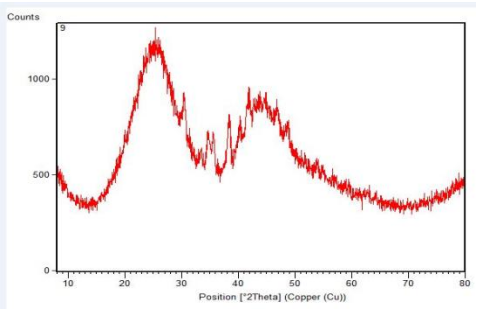

CSC/NiO

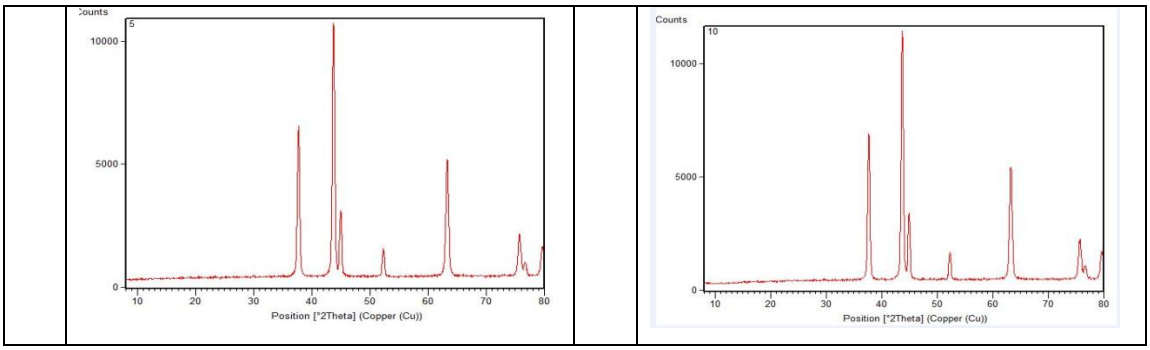

Figure 3 XRD diffractogram adsorbents (a) before (b) after adsorption process for CIP respectively.

The SEM micrographs in Figure 4 shows modified coconut shell adsorbents before and after CIP adsorptions. The adsorbents have a flat shape with semi-porous surface homogeneity with good grain distribution. After treatment they become rough due to cubic nanoparticles. The porous surface structures offer a strong chance for CIP adsorption (Falyouna et al., 2022).

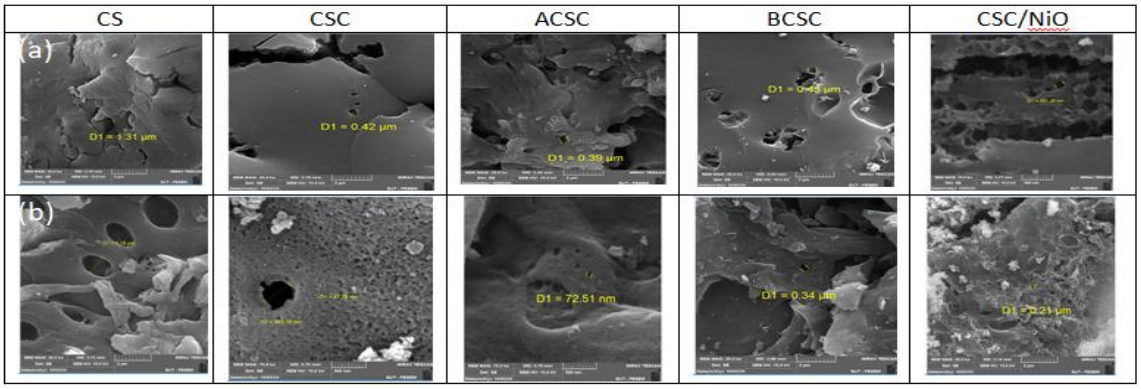

Figure 4 SEM micrographs of adsorbents (a) before (b) after adsorption processes for CIP respectively.

The EDX results in Figure 5 indicate successful synthesis of the CSC/NiO nanocomposite with surface adsorbents with an average size of 34 nm, indicating the successful adsorption of CIP (Wakejo et al., 2022).

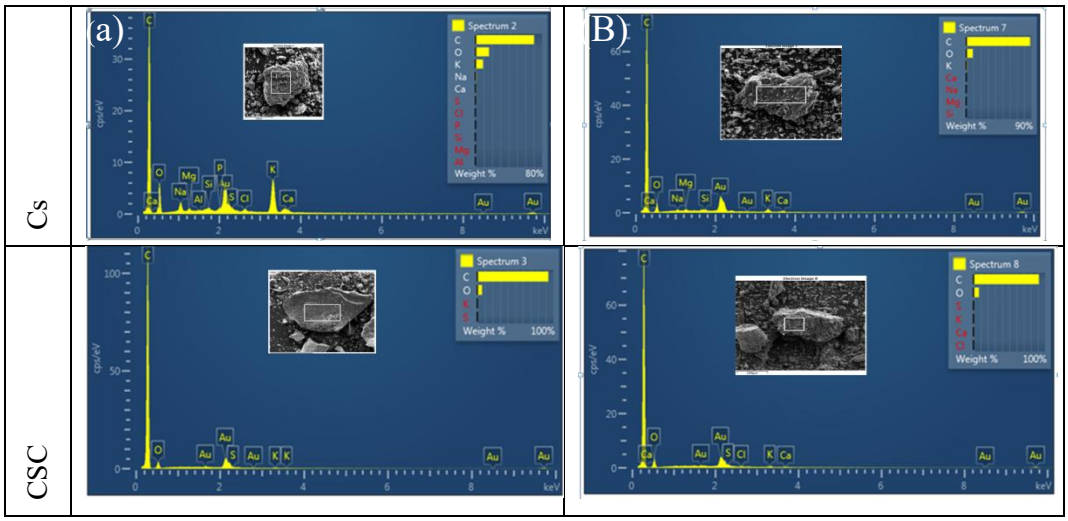

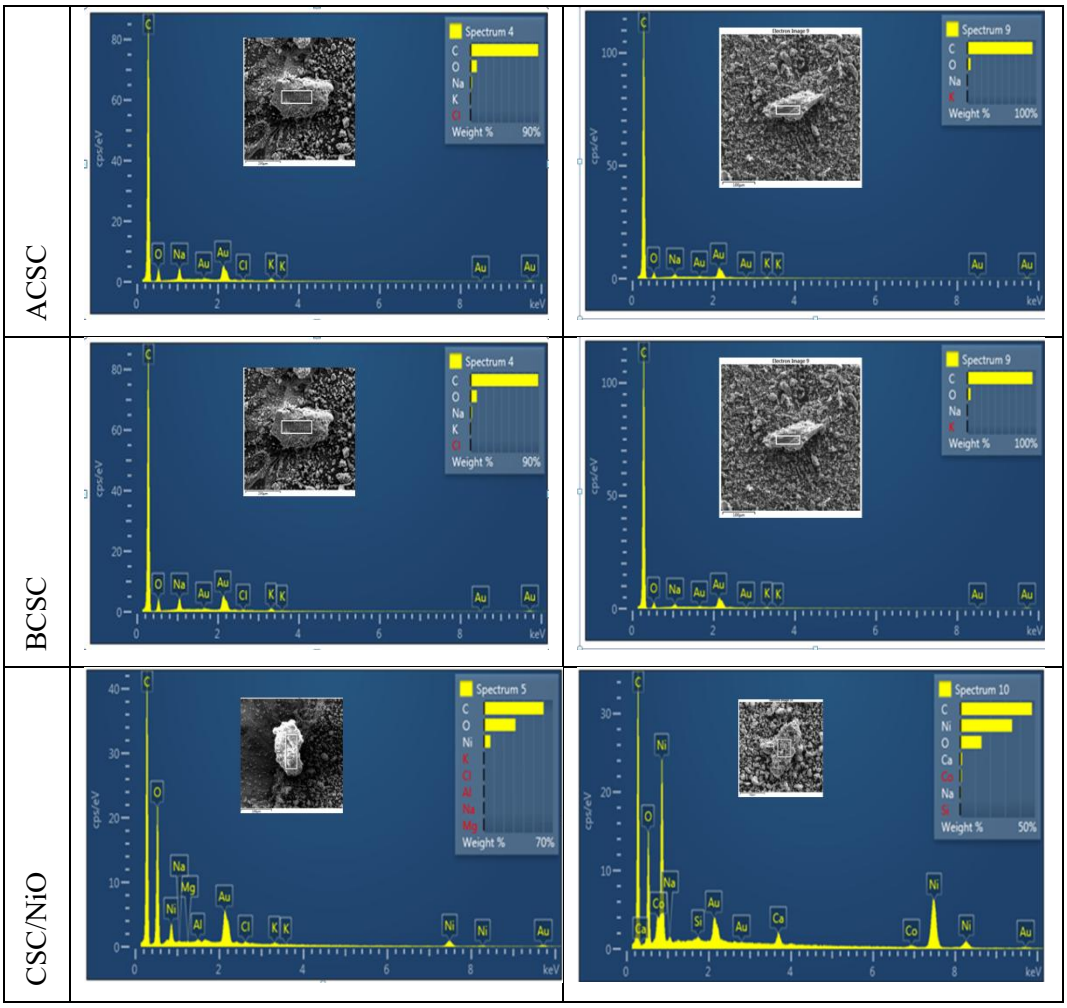

Figure 5 EDX micrographs of adsorbents (a) before (b) after adsorption for CIP respectively with gold coatings for surface microporous structure analysis.

3.2. Effect of initial concentration:

Figure 6 (a) demonstrates the effectiveness of adsorption on modified coconut shell adsorbents, using different initial concentrations of CIP. The q_e values were 71.34, 75.41, 78.71, 82.25 and 84.65 mg g^{-1} respectively, indicating that the goodness of adsorbent to adsorb CIP in aqueous solution (Bhagat et al., 2020).

3.3. Effect of pH.

Figure 6 (b) demonstrate the effect of pH on the modified coconut shell adsorbents to adsorb CIP. The CIP can exist in three forms: mono-cationic at pH 6, zwitterion at pH 6-9 and anionic at pH 9. At pH 7 CIP reached the highest efficiency. The percentages of adsorbed CIP for initial concentration 10 mgL^{-1} were 66.81%, 71.06%, 77.33%, 80.60% and 85.34% respectively. The interaction through adsorbent surface likely involve complexation or hydrogen bonding and electrostatically with the CIP (Pei et al., 2010).

3.4. Effect of Dosage

Figure 6 (c) demonstrates the effect of adsorbent dosage on the removal of CIP from aqueous solution. The percentages of adsorbed CIP were 49.68%, 52.90%, 54.99%, 58.06% and 60.31% respectively. The percentage of adsorbed CIP was found to be higher at higher dosages with removal remaining constant until the adsorbent and CIP reach equilibrium (Hoang et al., 2020).

3.5. Effect of contact time

Figure 6 (d) demonstrates the effect of contact time on the adsorption of CIP on various modified coconut shell adsorbents. The adsorption process reached equilibrium gradually due to the occupancy of active sites. The percentages of adsorbed CIP were 53.38%, 54.99%, 57.29%, 60.74% and 62.60% respectively. The initial quick adsorption was due to the large number of sites on the adsorbents surface but as the number decreased the

adsorption rate stabilized (Aljeboree et al., 2017).

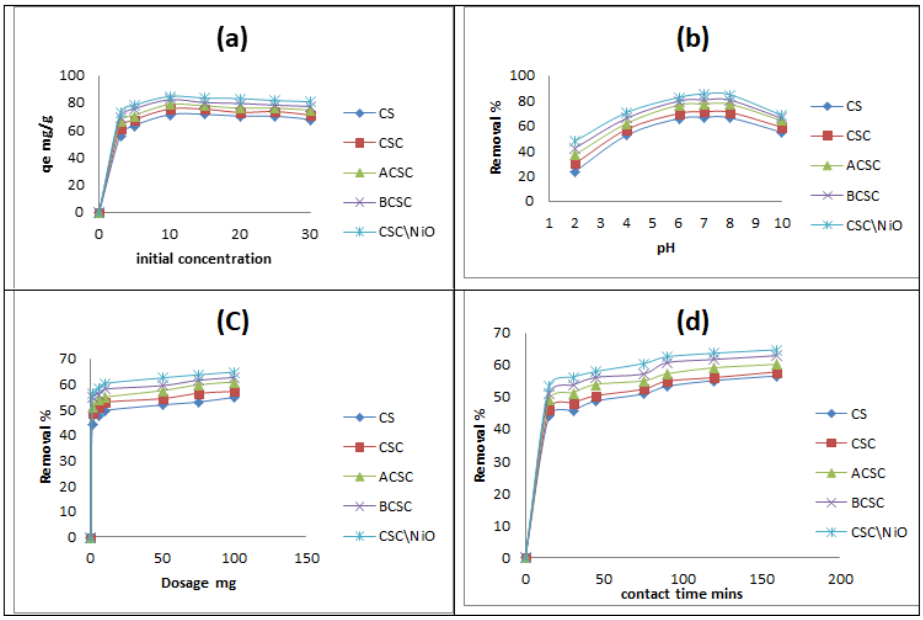

Figure 6 Effect of (a) initial concentration (b) pH, (c) dosage and (d) contact time for a removal efficiency for CIP (at the initial concentration of 10 mg L^{-1}, contact time of 160 min and dosage (0.01g, pH 7) by adsorbents at the 298 K.

3.5. Adsorption Kinetic Study

The kinetic study of CIP adsorption onto modified coconut shell adsorbents at different temperatures 298 K, 308 K and 318 K were analyzed by using kinetic models which is common to use in solid liquid adsorption process: the pseudo-first-order equation (Rahdar et al., 2019a), pseudo second - order equation (Dube et al., 2018) and Elovich kinetic models (Ashiq et al., 2019) as written in following equations.

Pseudo first-order; $$\log(q_e - q_t) = \log q_e - \frac{k_1 t}{2.303} \quad (4)$$

Pseudo second-order; $$\frac{t}{q_t} = \frac{1}{k_2 q_e^2} + \frac{t}{q_e} \quad (5)$$

Elovich; $$q_t = \frac{1}{\beta}\ln(\alpha\beta) + \frac{1}{\beta}\ln t \quad (6)$$

Figure 7 (a) and table 2,3 and 4 shows the adsorption of CIP at different temperatures and concentrations, determining the pseudo first order rate constant (k_1) and q_e and R^2 values. The experimental results differed from the calculated values, indicating that the adsorption process does not follow first order kinetics (Wakejo et al., 2022, Rahdar et al., 2019a).

Figure 7 (b) and table 2.3 and 4 demonstrated the second order rate constant (k_2) and q_e values were determined from a plot. The linearity of the plot and alignment of experimental and calculated q_e values were crucial for applying second order kinetics to the analyzed data (Dube et al., 2018).

The Figure 7 (c) shows The Elovich kinetic model constants, α and β are used to plot the initial adsorption rate and adsorption by adsorbents. The values for α, β, and R^2 ranged from 1.061 to 4.695 mg g^{-1} min^{-1}, 0.065 to 2.346 g mg^{-1}, and 0.725 to 0.993, respectively (Ashiq et al., 2019).

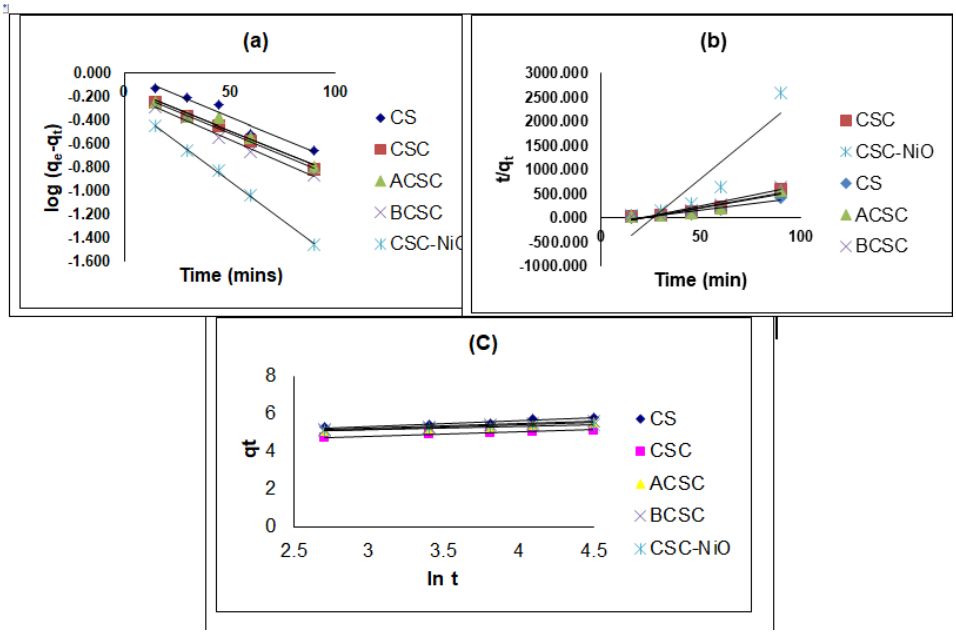

Figure 7 (a) Pseudo first order kinetic, (b) Pseudo second order kinetic and (c) Elovich model for the adsorption for CIP using adsorbents at 298 K.

Table 2 Pseudo (first, second) order the rate constants and Elovich for the adsorption on CIP on adsorbents at 298K.

Adsorbent	Conc.	Pseudo first order rate			Pseudo second order rate			Elovich		
		K_1 min^{-1}	q_e mg g^{-1}	R^2	K_2 g μg^{1} min^{-1}	q_e mg g^{-1}	R^2	A mg g^{-1} min^{-1}	B g mg^{-1}	R^2
CS	3	0.009	2.487	0.933	0.833	0.062	0.951	1.461	0.144	0.970
	5	0.007	1.023	0.965	0.294	0.169	0.932	2.168	0.297	0.935
	10	0.008	1.008	0.954	0.273	0.187	0.937	1.171	0.304	0.921
	15	0.008	2.259	0.886	0.144	0.300	0.861	1.231	0.558	0.725
CSC	3	0.008	1.822	0.979	0.518	0.090	0.885	1.785	0.161	0.969
	5	0.007	1.665	0.979	0.370	0.133	0.916	1.489	0.186	0.983
	10	0.008	1.358	0.997	0.371	0.133	0.917	1.134	0.226	0.986
	15	0.007	1.328	0.995	0.392	0.124	0.918	1.066	0.227	0.973
ACSC	3	0.011	1.465	0.933	0.769	0.050	0.802	2.851	0.180	0.937
	5	0.007	1.639	0.931	0.404	0.124	0.883	1.296	0.182	0.935
	10	0.007	1.320	0.965	0.349	0.139	0.901	1.117	0.218	0.932
	15	0.007	1.282	0.936	0.314	0.154	0.882	1.063	0.208	0.890
BSC	3	0.009	1.873	0.961	0.628	0.078	0.939	2.890	0.180	0.930
	5	0.009	1.517	0.996	0.552	0.083	0.907	1.415	0.215	0.984
	10	0.008	1.475	0.991	0.428	0.119	0.938	1.117	0.221	0.981
	15	0.008	1.417	0.995	0.414	0.119	0.928	1.073	0.225	0.979
CSC-NiO	3	0.020	1.216	0.901	4.356	0.008	0.706	1.606	0.431	0.988
	5	0.019	1.289	0.924	3.372	0.010	0.718	1.279	0.165	0.990
	10	0.013	1.031	0.999	1.306	0.030	0.840	1.094	0.181	0.997
	15	0.010	1.024	0.945	0.802	0.059	0.925	1.061	0.201	0.953

Table 3 Pseudo (first, second) order the rate constants and Elovich, for adsorption of CIP on adsorbents at 308K.

Adsorbent	Conc.	Pseudo first order rate			Pseudo second order rate			Elovich		
		K_1 min^{-1}	q_e mg g^{-1}	R^2	K_2 g μg^1 min^{-1}	q_e mg g^{-1}	R^2	A mg g^{-1} min^{-1}	B g mg^{-1}	R^2
CS	3	0.009	1.776	0.978	0.619	0.074	0.909	2.256	0.171	0.924
	5	0.010	1.351	0.983	0.548	0.078	0.877	1.608	0.218	0.947
	10	0.009	1.330	0.993	0.455	0.099	0.898	1.126	0.230	0.970
	15	0.008	1.351	0.996	0.391	0.124	0.915	1.070	0.226	0.975
CSC	3	0.005	3.720	0.887	0.824	0.084	0.973	1.255	0.082	0.943
	5	0.008	1.600	0.970	0.456	0.113	0.949	1.768	0.200	0.945
	10	0.007	1.483	0.854	0.384	0.176	0.973	1.195	0.244	0.954
	15	0.007	1.064	0.990	0.261	0.207	0.934	1.106	0.298	0.996
ACSC	3	0.005	3.590	0.933	0.603	0.116	0.969	1.186	0.065	0.840
	5	0.005	3.107	0.957	0.694	0.082	0.915	1.111	0.083	0.937
	10	0.004	2.262	0.889	0.465	0.169	0.980	1.061	0.123	0.941
	15	0.005	2.001	0.950	0.398	0.179	0.974	1.042	0.135	0.956
BSC	3	0.011	1.720	0.961	0.867	0.046	0.843	3.060	0.159	0.907
	5	0.009	1.530	0.962	0.523	0.090	0.926	1.464	0.202	0.925
	10	0.007	1.555	0.915	0.401	0.148	0.969	1.117	0.210	0.940
	15	0.007	1.397	0.918	0.369	0.160	0.968	1.082	0.242	0.964
CSC-NiO	3	0.010	15.03	0.913	6.022	0.009	0.959	1.050	0.026	0.968
	5	0.014	2.824	0.935	2.374	0.016	0.806	1.072	0.087	0.866
	10	0.013	2.143	0.952	1.325	0.033	0.925	1.095	0.174	0.967
	15	0.008	1.660	0.989	9.521	0.105	0.903	1.071	0.178	0.970

Table 4 Pseudo (first, second) order the rate constants and Elovich for the adsorption of CIP on adsorbents at 318K.

Adsorbent	Conc.	Pseudo first order rate			Pseudo second order rate			Elovich		
		K min^{-1}	q_e mg g^{-1}	R^2	K_2g μg^1 min^{-1}	q_e mg g^{-1}	R^2	A mg g^{-1} min^{-1}	B g mg^{-1}	R^2
CS	3	0.007	2.535	0.964	0.655	0.086	0.966	1.733	0.130	0.975
	5	0.008	1.510	0.938	0.446	0.123	0.964	2.174	0.232	0.974
	10	0.006	1.287	0.989	0.275	0.204	0.931	1.141	0.214	0.962
	15	0.006	1.232	0.997	0.259	0.238	0.960	1.096	0.229	0.980
CSC	3	0.008	3.263	0.948	0.935	0.052	0.921	1.383	0.088	0.873
	5	0.007	1.889	0.889	0.510	0.119	0.970	1.818	0.182	0.946
	10	0.007	1.237	0.995	0.333	0.149	0.915	1.221	0.244	0.973
	15	0.007	1.134	0.976	0.303	0.160	0.893	1.102	0.254	0.953
ACSC	3	0.008	1.772	0.988	0.655	0.080	0.947	2.928	0.144	0.997
	5	0.007	2.499	0.993	0.528	0.098	0.931	1.367	0.170	0.999
	10	0.007	5.078	0.988	0.493	0.122	0.968	1.102	0.185	0.961
	15	0.007	9.954	0.975	0.411	0.122	0.927	1.101	0.283	0.852
BSC	3	0.009	1.899	0.992	0.650	0.069	0.893	4.695	0.161	0.965
	5	0.008	1.906	0.979	0.520	0.095	0.905	1.391	0.165	0.982
	10	0.007	1.637	0.974	0.405	0.142	0.958	1.122	0.205	0.993

	15	0.006	1.393	0.993	0.327	0.161	0.922	1.072	0.207	0.974
CSC-NiO	3	0.016	1.837	0.876	2.082	0.019	0.890	1.081	0.179	0.928
	5	0.008	1.300	0.983	0.930	0.043	0.873	1.336	1.097	0.927
	10	0.014	1.233	0.976	0.374	0.139	0.949	1.132	1.095	0.854
	15	0.004	1.309	0.996	0.246	0.286	0.963	1.220	2.346	0.954

3.6. Adsorption Isotherm Study.

To examine the interactions between CIP and various modified coconut shell adsorbents at different temperatures 298K, 308K and 318K using the Freundlich isotherm model (Rahdar et al., 2019b), Langmuir (Dhiman and Sharma, 2019) and Temkin (Zhang et al., 2019), to evaluate the equilibrium CIP adsorption isotherm using those following Equations.

Freundlich;

$$\ln q_e = \ln k_F + \frac{1}{n} \ln c_e \quad (7)$$

Langmuir

$$\frac{C_e}{q_e} = \frac{1}{K_L q_e} + \frac{C_e}{q_m} \quad (8)$$

$$R_L = \frac{1}{1 + K_L C_o} \quad (9)$$

Temkin;

$$q_e = \beta \ln K_T + \beta \ln C_e \quad (10)$$

The Figure 8 (a) and table 5,6 and 7 shows the Freundlich constant K_F, n_F and R^2 values for CIP loaded on an adsorbent, revealing their values within the range of 3.05-3.694 mgg^{-1}, 1.379-1.720 and 0.886-0.990 respectively.

Figure 8 (b) and table 5,6 and 7 shows the Langmuir isotherm for the adsorption of CIP on the adsorbents. It involves a linear relationship between the equilibrium concentrations of CIP, the amount of CIP adsorbed per unit mass of adsorbent. The results shows that CIP adsorption follows the Langmuir isotherm at different temperatures. The best match for CIP adsorption is the monolayer of CIP molecules on the adsorbent surface.

Figure 8 (c) and table 5,6 and 7 shows the Temkin equilibrium binding constants K_T and β. Values of K_T, β and R^2 ranged between 2.074-4.726 L g^{-1}, 2144-11680 J mol^{-1} and 0.918-0.999 with Temkin isotherm parameters recorded at different temperatures (298, 308, and 318) K. The Adsorption process of CIP was governed by the specific adsorption sites and by a complex process including ion exchange, surface precipitation, surface complexation and physical Biosorption due to Van der Waals force. External diffusion and internal diffusion or transport into the adsorbent particle, finally adsorption to reach saturation.

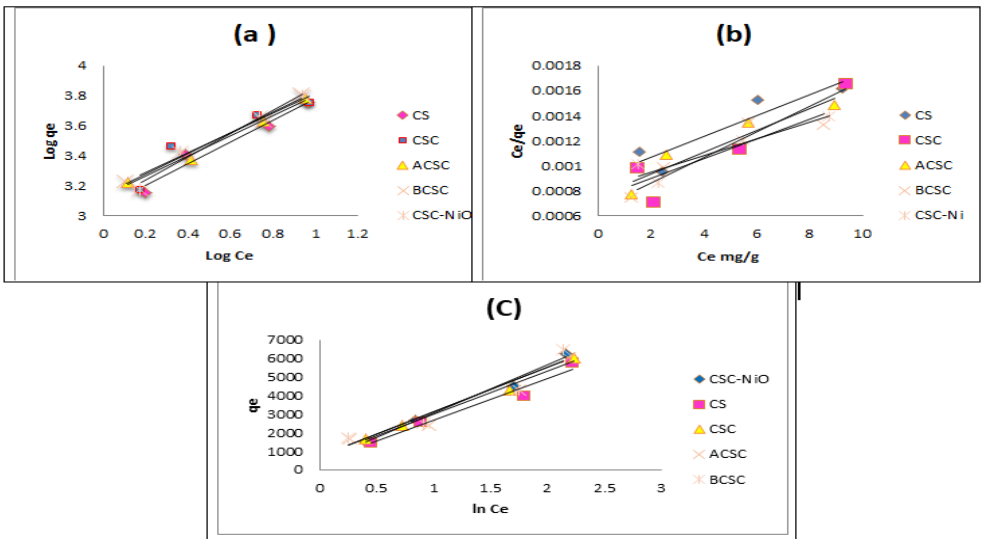

Figure 8 (a) Freundlich, (b) Langmuir and (c) Temkin model, for an adsorption of the CIP using adsorbents at 298 K

Table 5 parameters of Adsorption Isotherm for the different models Freundlich, Temkin and Langmuir for CIP using adsorbents at 298 K.

model	Parameter	CS	CSC	ACSC	BCSC	CSC-NiO
Freundlich	K_F(mg g^{-1})	3.056	3.159	3.132	3.145	3.532
	n_F	1.379	1.527	1.500	1.615	1.555
	R^2	0.961	0.886	0.992	0.988	0.971
Langmuir	K_L (L mg^{-1})	0.09	0.143	0.113	0.011	0.088
	C_m(µg g^{-1})	12500	10000	11111	12500	14286
	R_L	0.526	0.412	0.471	0.897	0.533
	R^2	0.845	0.864	0.899	0.827	0.871
Temkin	K_T (l g^{-1})	1.494	2.910	2.112	2.042	1.452
	β (J $mol^{-1)}$	2253	2144	11250	2381	2603
	R^2	0.964	0.999	0.944	0.920	0.989

Table 6 parameters of Adsorption Isotherm for the models Freundlich, Temkin and Langmuir for CIP using adsorbents at 308 K.

model	parameter	CS	CSC	ACSC	BCSC	CSC-NiO
Freundlich	K_F(mg/g)	3.175	3.241	3.157	3.230	3.608
	n_F	1.54	1.455	1.436	1.618	1.646
	R^2	0.930	0.906	0.990	0.988	0.973
Langmuir	K_L (L mg^{-1})	0.130	0.160	0.114	0.150	0.133
	C_m(µg g^{-1})	11111	12500	12500	11111	12500
	R_L	0.435	0.385	0.467	0.400	0.429
	R^2	0.934	0.861	0.858	0.878	0.980

Temkin	K_T (l g^{-1})	2.751	3.300	2.074	3.531	2.676
	β (J mol^{-1})	2231	2603	11680	2285	2453
	R^2	0.971	0.977	0.934	0.952	0.983

Table 7 the parameters of Adsorption Isotherm for the models Temkin, Freundlich and Langmuir for CIP using adsorbents at 318 K.

mod.	parameter	CS	CSC	ACSC	BCSC	CSC-NiO
Freundlich	K_F(mg g^{-1})	3.260	3.313	3.270	3.275	3.694
	n_F	1.40	1.045	1.698	1.637	1.720
	R^2	0.971	0.957	0.988	0.993	0.955
Langmuir	K_L (L mg^{-1})	0.120	0.175	0.180	0.180	0.160
	C_m(µg g^{-1})	16667	14285	11111	11111	12500
	R_L	0.455	0.364	0.357	0.357	0.385
	R^2	0.760	0.939	0.894	0.928	0.926
Temkin	K_T (l g^{-1})	2.823	3.936	4.726	4.429	4.044
	β (J mol^{-1})	2955	2947	11098	2368	2502
	R^2	0.918	0.971	0.928	0.950	0.963

3.7. Thermodynamic Study of Adsorption:

The thermodynamic study was conducted on the removal of CIP by various adsorbents, assessing Gibbs free energy change (ΔG^o), enthalpy change (ΔH^o) and entropy change (ΔS^o) using Van't Hoff equation (Balarak et al., 2021).

$$\Delta G^o = -RT \ln K_o \quad (11)$$

$$LnK_o = \frac{\Delta S^o}{R} - \frac{\Delta H^o}{RT} \quad (12)$$

Where: T, R and K_0 are absolute temperature, universal gas constant and equilibrium thermodynamic constant respectively. Table 8 and Figure 9 demonstrated the values of K_o, E_a, ΔG^o, ΔH^o, ΔS^o and R^2 ranged from 1955–7914, 18.95-51.77 kJ mol^{-1}, -18.47 to -23.74 kJ mol^{-1}, 18.95-49.29 kJ mol^{-1}, 0.131-0.228 kJ mol^{-1} K^{-1}, 0.992-1 respectively. The ΔH^o positive value meant the endothermic nature process. When CIP ions were adsorbed onto all adsorbents, the ΔS^o positive value showed an increase in unpredictability at the solid/solution interface. The processes were spontaneous and ΔG^o was going to have a negative value as the temperature rose.

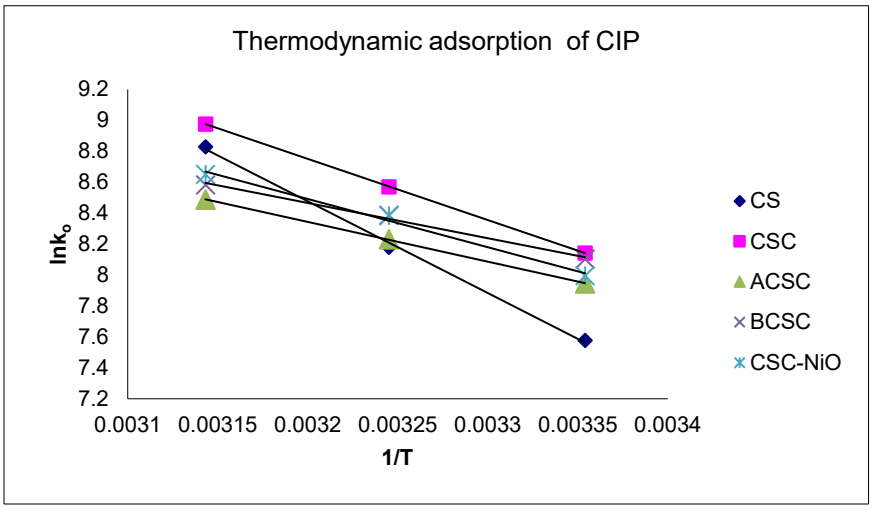

Figure 9 Variation of the ln K_o with the 1/T of adsorption of CIP on adsorbents.

Table 8 Changes in free energy, standard enthalpy and standard entropy for adsorption for CIP on the adsorbents at three different temperatures.

T/ K	Parameter	CS	CSC	ACSC	BCSC	CSC-NiO
289	K_o	1955	3438	2823	3306	2967
	ΔG (kJ mol^{-1})	-18.47	-19.85	-19.37	-19.75	-19.49
309	K_o	3565	5277	3757	4388	5720
	ΔG (kJ mol^{-1})	-20.95	-21.96	-21.09	-21.49	-22.17
318	K_o	6831	7914	4854	5342	4380
	ΔG (kJ mol^{-1})	-23.35	-23.74	-22.45	-22.70	-22.18
ΔH (kJ mol^{-1})		49.29	32.88	21.37	18.95	25.94
ΔS (kJ mol^{-1} K)		0.228	0.178	0.138	0.131	0.154
Ea (kJ mol^{-1})		51.77	35.36	23.85	21.43	28.42
R^2		0.998	1	1	0.993	0.992

4. Conclusions

Water and wastewater treatment is impotent to resume life so: the adsorbents in this study; CS, CSC, ACSC, BCSC and CSC/NiO nanocomposite, examined to extract CIP from a water-based solution. The findings showed that adsorbents are 20–25 nm in size and have a crystalline structure. The FTIR, XRD, SEM and EDX characterization data show that CIP was successfully adsorbed onto the adsorbents. The pseudo second-order Langmuir equation matches the maximum adsorption capacity and isotherm data rather well. The endothermic and spontaneous processes were validated by the thermodynamic parameters. In four successive cycles, the adsorbents regeneration demonstrated a high elimination of CIP from the aqueous solution.

Acknowledgements

We would like to thank Salahaddin University-Erbil, Kurdistan Region, Iraq for supporting this research.

References

AL-MUSAWI, T. J., MAHVI, A. H., KHATIBI, A. D. & BALARAK, D. 2021. Effective adsorption of ciprofloxacin antibiotic using powdered activated carbon magnetized by iron (III) oxide magnetic nanoparticles. *Journal of porous materials,* 28**,** 835-852.

ALJEBOREE, A. M., ALKAIM, A. F. & AL-DUJAILI, A. H. 2015. Adsorption isotherm, kinetic modeling and thermodynamics of crystal violet dye on coconut husk-based activated carbon. *Desalination and Water Treatment,* 53**,** 3656-3667.

ALJEBOREE, A. M., ALSHIRIFI, A. N. & ALKAIM, A. F. 2017. Kinetics and equilibrium study for the adsorption of textile dyes on coconut shell activated carbon. *Arabian journal of chemistry,* 10**,** S3381-S3393.

ALSAGER, O. A., ALNAJRANI, M. N., ABUELIZZ, H. A. & ALDAGHMANI, I. A. 2018. Removal of antibiotics from water and waste milk by ozonation: kinetics, byproducts, and antimicrobial activity. *Ecotoxicology and environmental safety,* 158**,** 114-122.

ASHIQ, A., ADASSOORIYA, N. M., SARKAR, B., RAJAPAKSHA, A. U., OK, Y. S. & VITHANAGE, M. 2019. Municipal solid waste biochar-bentonite composite for the removal of antibiotic ciprofloxacin from aqueous media. *Journal of environmental management,* 236**,** 428-435.

AYRILMIS, N., JARUSOMBUTI, S., FUEANGVIVAT, V., BAUCHONGKOL, P. & WHITE, R. H. 2011. Coir fiber reinforced polypropylene composite panel for automotive interior applications. *Fibers and polymers,* 12**,** 919-926.

AZIZI, A. 2021. Green synthesis of iron oxide/cellulose magnetic recyclable nanocomposite and its evaluation in ciprofloxacin removal from aqueous solutions. *Journal of the Iranian Chemical Society,* 18**,** 331-341.

BAIG, U., UDDIN, M. K. & GONDAL, M. 2020. Removal of hazardous azo dye from water using synthetic nano adsorbent: Facile synthesis, characterization, adsorption, regeneration and design of experiments. *Colloids and Surfaces A: Physicochemical and Engineering Aspects,* 584**,** 124031.

BALARAK, D., MAHVI, A. H., SHIM, M. J. & LEE, S.-M. 2021. Adsorption of ciprofloxacin from aqueous solution onto synthesized NiO: isotherm, kinetic and thermodynamic studies. *Desalin Water Treat,* 212**,** 390-400.

BHAGAT, C., KUMAR, M., TYAGI, V. K. & MOHAPATRA, P. K. 2020. Proclivities for prevalence and treatment of antibiotics in the ambient water: a review. *npj Clean Water,* 3**,** 42.

CHANG, L., PU, Y., JING, P., CUI, Y., ZHANG, G., XU, S., CAO, B., GUO, J., CHEN, F. & QIAO, C. 2021. Magnetic core-shell MnFe2O4@ TiO2 nanoparticles decorated on reduced graphene oxide as a novel adsorbent for the removal of ciprofloxacin and Cu (II) from water. *Applied Surface Science,* 541**,** 148400.

CHEN, T., LIU, H. & BIE, R. 2020. Temperature rise characteristics of coal-KOH adduct under microwave heating and the properties of resultant activated carbon for catalytic methane decomposition. *Journal of Analytical and Applied Pyrolysis,* 145**,** 104739.

DE ILURDOZ, M. S., SADHWANI, J. J. & REBOSO, J. V. 2022. Antibiotic removal processes from water & wastewater for the protection of the aquatic environment-a review. *Journal of water process engineering,* 45**,** 102474.

DHIMAN, N. & SHARMA, N. 2019. Batch adsorption studies on the removal of ciprofloxacin hydrochloride from aqueous solution using ZnO nanoparticles and groundnut (Arachis hypogaea) shell powder: a comparison. *Indian Chemical Engineer,* 61**,** 67-76.

DUBE, C., TANDLICH, R. & WILHELMI, B. 2018. Adsorptive removal of ciprofloxacin and isoniazid from aqueous solution.

FAKHRE, N. A. & IBRAHIM, B. M. 2018. The use of new chemically modified cellulose for heavy metal ion adsorption. *Journal of Hazardous Materials,* 343**,** 324-331.

FALYOUNA, O., MAAMOUN, I., BENSAIDA, K., TAHARA, A., SUGIHARA, Y. & ELJAMAL, O. 2022. Encapsulation of iron nanoparticles with magnesium hydroxide shell for remarkable removal of ciprofloxacin from contaminated water. *Journal of Colloid and Interface Science,* 605**,** 813-827.

HASSANI, A., KHATAEE, A., FATHINIA, M. & KARACA, S. 2018. Photocatalytic ozonation of ciprofloxacin from aqueous solution using TiO2/MMT nanocomposite: Nonlinear modeling and optimization of the process via artificial neural network integrated genetic algorithm. *Process Safety and Environmental Protection,* 116**,** 365-376.

HOANG, L. P., VAN, H. T., NGUYEN, T. T. H., NGUYEN, V. Q. & QUANG THANG, P. 2020. Coconut shell activated carbon/CoFe2O4 composite for the removal of rhodamine B from aqueous solution. *Journal of Chemistry,* 2020**,** 9187960.

IBRAHIM, B. M. & FAKHRE, N. A. 2019. Crown ether modification of starch for adsorption of heavy metals from synthetic wastewater. *International Journal of Biological Macromolecules,* 123**,** 70-80.

IBRAHIM, B. M., FAKHRE, N. A., JALHOOM, M. G., QADER, I. N., SHAREEF, H. Y. & JALAL, A. F. 2024. Removal of lead ions from aqueous solutions by modified cellulose. *Environmental Technology,* 45**,** 2335-2347.

IGWEGBE, C. A., OBA, S. N., ANIAGOR, C. O., ADENIYI, A. G. & IGHALO, J. O. 2021. Adsorption of ciprofloxacin from water: a comprehensive review. *Journal of Industrial and Engineering Chemistry,* 93**,** 57-77.

JIANG, W.-T., CHANG, P.-H., WANG, Y.-S., TSAI, Y., JEAN, J.-S., LI, Z. & KRUKOWSKI, K. 2013. Removal of ciprofloxacin from water by birnessite. *Journal of Hazardous Materials,* 250**,** 362-369.

KUŚMIEREK, K., ŚWIĄTKOWSKI, A., SKRZYPCZYŃSKA, K., BŁAŻEWICZ, S. & HRYNIEWICZ, J. 2017. The effects of the thermal treatment of activated carbon on the phenols adsorption. *Korean Journal of Chemical Engineering,* 34**,** 1081-1090.

MALAKOOTIAN, M., NASIRI, A. & MAHDIZADEH, H. 2018. Preparation of CoFe2O4/activated carbon@ chitosan as a new magnetic nanobiocomposite for

adsorption of ciprofloxacin in aqueous solutions. *Water Science and Technology,* 78**,** 2158-2170.

NAMASIVAYAM, C., KUMAR, M. D., SELVI, K., BEGUM, R. A., VANATHI, T. & YAMUNA, R. 2001. 'Waste'coir pith—a potential biomass for the treatment of dyeing wastewaters. *Biomass and Bioenergy,* 21**,** 477-483.

PANAHI, H. K. S., DEHHAGHI, M., OK, Y. S., NIZAMI, A.-S., KHOSHNEVISAN, B., MUSSATTO, S. I., AGHBASHLO, M., TABATABAEI, M. & LAM, S. S. 2020. A comprehensive review of engineered biochar: production, characteristics, and environmental applications. *Journal of Cleaner Production,* 270**,** 122462.

PATRA, G., BARNWAL, R., BEHERA, S. K. & MEIKAP, B. 2018. Removal of dyes from aqueous solution by sorption with fly ash using a hydrocyclone. *Journal of Environmental Chemical Engineering,* 6**,** 5204-5211.

PEI, Z., SHAN, X.-Q., KONG, J., WEN, B. & OWENS, G. 2010. Coadsorption of ciprofloxacin and Cu (II) on montmorillonite and kaolinite as affected by solution pH. *Environmental science & technology,* 44**,** 915-920.

PENG, X., HU, F., HUANG, J., WANG, Y., DAI, H. & LIU, Z. 2016. Preparation of a graphitic ordered mesoporous carbon and its application in sorption of ciprofloxacin: Kinetics, isotherm, adsorption mechanisms studies. *Microporous and Mesoporous Materials,* 228**,** 196-206.

PENG, X., HU, F., ZHANG, T., QIU, F. & DAI, H. 2018. Amine-functionalized magnetic bamboo-based activated carbon adsorptive removal of ciprofloxacin and norfloxacin: A batch and fixed-bed column study. *Bioresource technology,* 249**,** 924-934.

RAHDAR, A., RAHDAR, S., AHMADI, S. & FU, J. 2019a. Adsorption of ciprofloxacin from aqueous environment by using synthesized nanoceria. *Ecological Chemistry and Engineering S,* 26**,** 299-311.

RAHDAR, S., RAHDAR, A., IGWEGBE, C. A., MOGHADDAM, F. & AHMADIA, S. 2019b. Synthesis and physical characterization of nickel oxide nanoparticles and its application study in the removal of ciprofloxacin from contaminated water by adsorption: equilibrium and kinetic studies. *Desalination and water treatment,* 141**,** 386-393.

RUMMAN, G. A., AL-MUSAWI, T. J., SILLANPAA, M. & BALARAK, D. 2021. Adsorption performance of an amine-functionalized MCM–41 mesoporous silica nanoparticle system for ciprofloxacin removal. *Environmental Nanotechnology, Monitoring & Management,* 16**,** 100536.

SAMARGHANDI, M. R., ASGARI, G., SHOKOOHI, R., DARGAHI, A. & ARABKOUHSAR, A. 2019. Removing amoxicillin antibiotic from aqueous solutions by Saccharomyces cerevisiae bioadsorbent: kinetic, thermodynamic and isotherm studies. *Desalination and Water Treatment,* 152**,** 306-315.

SHAREF, H. Y., JALAL, A. F., IBRAHIM, B. M., FAKHRE, N. A. & QADER, I. N. 2023. New ion-imprinted polymer for selective removal of Cu2+ ion in aqueous solution using extracted Aloe vera leaves as a monomer. *International Journal of Biological Macromolecules,* 239**,** 124318.

SOUSA NETO, V. D. O., CARVALHO, T. V., HONORATO, S. B., GOMES, C. L., BARROS, F. C. F., FREIRE, P. T. & NASCIMENTO, R. F. 2012. Coconut bagasse treated by thiourea/ammonia solution for cadmium removal: kinetics and adsorption equilibrium. *BioResources,* 7.

SU, W., ZHOU, L. & ZHOU, Y. 2003. Preparation of microporous activated carbon from coconut shells without activating agents. *Carbon,* 41**,** 861-863.

SUN, J., XU, F., SUN, X., XIAO, B. & SUN, R. 2005. Physico-chemical and thermal characterization of cellulose from barley straw. *Polymer Degradation and stability,* 88**,** 521-531.

WAKEJO, W. K., MESHASHA, B. T., KANG, J. W. & CHEBUDE, Y. 2022. Enhanced ciprofloxacin removal from aqueous solution using a chemically modified biochar derived from bamboo sawdust: adsorption process optimization with response surface methodology. *Adsorption Science & Technology,* 2022**,** 2699530.

WANG, G., XU, J., SUN, Z. & ZHENG, S. 2020. Surface functionalization of montmorillonite with chitosan and the role of surface properties on its adsorptive performance: a comparative study on mycotoxins adsorption. *Langmuir,* 36**,** 2601-2611.

YAHYA, M. A., AL-QODAH, Z. & NGAH, C. Z. 2015. Agricultural bio-waste materials as potential sustainable precursors used for activated carbon production: A review. *Renewable and sustainable energy reviews,* 46**,** 218-235.

YAHYA, M. S., OTURAN, N., EL KACEMI, K., EL KARBANE, M., ARAVINDAKUMAR, C. & OTURAN, M. A. 2014. Oxidative degradation study on antimicrobial agent ciprofloxacin by electro-Fenton process: kinetics and oxidation products. *Chemosphere,* 117**,** 447-454.

ZHANG, J., KHAN, M. A., XIA, M., ABDO, A. M., LEI, W., LIAO, C. & WANG, F. 2019. Facile hydrothermal synthesis of magnetic adsorbent CoFe 2 O 4/MMT to eliminate antibiotics in aqueous phase: tetracycline and ciprofloxacin. *Environmental Science and Pollution Research,* 26**,** 215-226.

ZHANG, L., RUAN, D. & GAO, S. 2002. Dissolution and regeneration of cellulose in NaOH/thiourea aqueous solution. *Journal of Polymer Science Part B: Polymer Physics,* 40**,** 1521-1529.

ZHENG, X., HE, X., PENG, H., WEN, J. & LV, S. 2021. Efficient adsorption of ciprofloxacin using Ga2S3/S-modified biochar via the high-temperature sulfurization. *Bioresource Technology,* 334**,** 125238.

ZHU, K., SHEN, Y., HOU, J., GAO, J., HE, D., HUANG, J., HE, H., LEI, L. & CHEN, W. 2021. One-step synthesis of nitrogen and sulfur co-doped mesoporous graphite-like carbon nanosheets as a bifunctional material for tetracycline removal via adsorption and catalytic degradation processes: Performance and mechanism. *Chemical Engineering Journal,* 412**,** 128521.